VIBRATION TESTING AND ANALYSIS OF THE PICKUP HEADER OF STRAW FORAGE HARVESTER UNDER MULTI-SOURCE EXCITATION

/

秸秆饲料收获机捡拾割台在多源激励下的振动试验与分析

Qiaofei MU[1,2], Haiqing TIAN*[1,2], Ziqing XIAO[1,2], Chunxiang ZHUO[1,2], Xiaoyu XUE[1,2], Leifeng TANG[1,2]

[1)] Inner Mongolia Agricultural University, College of Mechanical and Electrical Engineering, Hohhot/China;

[2)] Inner Mongolia Engineering Research Centre of Intelligent Equipment for the Entire Process of Forage and Feed Production, Hohhot 010018, China;

Tel: 15947019846; E-mail: 2022202050021@emails.imau.cn; hqtian@126.com

DOI: https://doi.org/10.35633/inmateh-73-27

Keywords: *Agricultural machinery; Pick-up header; Multi-source excitation; operational transfer path analysis*

ABSTRACT

The complex vibration field in agricultural equipment during field operations not only predisposes key mechanical components to fatigue failure, but also leads to crop losses. This study introduces the Operating Transfer Path Analysis (OTPA) method to identify the vibration sources in the pickup header of a straw forage harvester. Finite element modal analysis, vibration testing, and operating transfer path analysis were conducted on the header frame. The findings indicate that excitation sources, including the hammer claw device, transmission, and dust box on the pickup header, are prone to resonant coupling with the header frame. The analysis reveals that the right transmission output shaft contributes 18.3% to the vertical vibrations on the right side panel of the frame. Meanwhile, the left transmission output shaft accounts for 29.4% of the horizontal vibrations on the left side panel. Additionally, the transmission input end is responsible for 54.8% of the horizontal vibrations on the front beam, while the dust box end contributes 45% to the forward vibrations on the rear beam. By identifying the primary transmission paths, the most effective strategies for the vibration reduction and optimization design of the pickup header can be developed. Furthermore, this study offers a theoretical foundation and experimental references for the vibration reduction optimization of other agricultural machinery.

摘要

农业装备在田间收获作业时复杂的振动场不仅易导致机械关键部件疲劳破坏，还会造成农作物收获损失。本研究引入工况传递路径分析方法（OTPA）作为识别秸秆饲料收获机捡拾割台振动原因的手段。对割台机架进行有限元模态分析、振动试验分析和工况传递路径分析。结果表明：捡拾割台上锤爪装置、变速箱以及除尘箱体等激励源易与割台机架发生共振耦合。其中，变速箱右输出端对机架右侧板竖直方向上振动贡献占比 18.3%；变速箱左输出端对机架左侧板水平方向上振动贡献占比 29.4%；变速箱输入端对机架前梁水平方向上振动贡献占比54.8%；除尘箱体轴承端对机架后梁前进方向上振动贡献占比45%。通过确定主要的传递路径，可为捡拾割台的减振优化设计制定最有效的改进方案。同时，本研究可为其他农业装备的减振优化提供理论依据和试验参考。

INTRODUCTION

Crop straw, as an important agricultural by-product, has received much attention in recent years globally, especially in China (*Lu et al., 2014; McKendry et al., 2002*). Yellow storage feed harvesting equipment integrates operations such as cutting, picking up, dust removal, and baling of crop straw into a seamless process that converts the straw into filamentous material for livestock use, significantly enhancing straw resource utilization efficiency (*Awad et al.,2022; El Ghobashy et al., 2023*).

During operation, the yellow silage harvesting equipment experiences significant vibration due to the road surface excitation and the concurrent functioning of multiple components. According to relevant data, 80% of mechanical structure damage is attributed to fatigue, while 75% is related to vibration (*Yao, and Y et al., 2020; An et al., 2020; Lai, S, and P et al., 2018*). To address the vibration issues in agricultural harvesting equipment and mitigate vibration intensity, numerous scholars have undertaken related research.

Scholars have integrated modal analysis with experimental validation to optimize structures by shifting their natural frequencies away from the range of external excitation forces. For example, Jiang and colleagues enhanced the frame structure of a rapeseed cutting and drying machine using finite element analysis. By tuning the frame's natural frequency to circumvent resonance, they performed a finite element static analysis on the optimized structure (*Jiang et al., 2017*). Scholars have integrated theoretical calculations, experimental computations, and simulation analysis to mitigate the risk of resonance in agricultural equipment. Through structural optimization, they successfully isolated external excitation frequencies, thereby achieving significant vibration reduction and overall optimization (*Chen et al., 2020*). In summary, most scholars primarily employ methods such as vibration testing and simulation analysis to optimize and improve the damaged parts of harvesting equipment, with the main research focusing on the establishment of vibration models (*Nakata, Yuji, and Takao et al., 2010*), vibration and comfort analysis of cab seats (*Ahmadian, Seyed, and Barat et al., 2014*), and vibration of cutter knives and cutting tables (*Chuan-Udom et al., 2017; Chen, Han, Lu et al., 2012*).

In fact, agricultural harvesting equipment is subject to dynamic loads from various sources of excitation during operation. The vibrations from different sources can create complex vibrational couplings, leading to intense vibrations throughout the machinery (*Harikrishnan, and Varun et al., 2017*). Therefore, in order to more precisely reduce vibration and noise in agricultural harvesting equipment, it is necessary to obtain the vibration characteristics of each excitation source in the harvesting equipment, as well as the vibration transmission paths and their contributions.

Operating Transfer Path Analysis (OTPA) serves as an essential tool for analysing the transmission of structural vibrations and noise. It is routinely employed to assess the vibrational contributions of various transfer paths, aiming to pinpoint the primary paths responsible for vibration (*Chen et al., 2023*). Researchers have utilized the OTPA method in the automotive industry, with De Klerk et al. employing it to investigate tire vibration noise and assess the influence of structural and acoustic pathways on noise at specific points (*De, Alexander et al., 2010*). Moreover, the OTPA method has been employed in the agricultural machinery sector. Notably, Qi Quan and his team applied the OTPA method to pinpoint structural noise sources within an excavator cabin. Through comparison of synthetic and actual measured signals, they confirmed the method's effectiveness (*Qi et al., 2017*). The Operational Transfer Path Analysis (OTPA) method has evolved over an extended period and found applications across various fields. However, the application of the OTPA method in agricultural straw harvesting equipment remains relatively uncommon, particularly in the domain of straw feed harvesting equipment research.

The study aims to conduct parametric modeling of the pickup header on the straw feed harvester. Modal analysis will be employed to determine the modal parameters of the frame. Additionally, field vibration tests on the pickup header have been conducted, analysing the header and its various working components under diverse operating conditions. Ultimately, the study utilizes the Operational Transfer Path Analysis (OTPA) method to analyse vibration test data under various working conditions. This analysis assesses the contributions of different transmission paths originating from the primary excitation sources under specified conditions. It identifies the primary excitation source and its transmission path affecting the pickup header frame, pinpointing the underlying cause of the frame's vibration and deformation. The anticipated results of this study are expected to offer a theoretical foundation and novel insights into developing strategies for vibration reduction and noise control in straw feed harvester pickup headers, as well as aiding the structural design and development of new models. Furthermore, these findings are crucial for fostering the rapid expansion of agricultural equipment and accelerating the development of agricultural mechanization globally.

MATERIAL AND METHODS

Finite element modeling of the pickup header

This paper examines the pickup header of a straw forage harvester. The pickup header frame model was constructed using SolidWorks (2018) 3D software. To accommodate finite element calculations and enhance finite element analysis efficiency, the model was suitably simplified.

The simplification scheme is as follows:

1. Ignore supports that have minimal impact on the structural stiffness and strength;
2. Disregard the effects of welding and bolted connections on the material properties of components;
3. Ignore small holes, chamfers, and other structures smaller than the mesh size that have a significant effect on finite element calculations but not a major impact on model quality.

The simplified frame of the pickup header is shown in Figure 1.

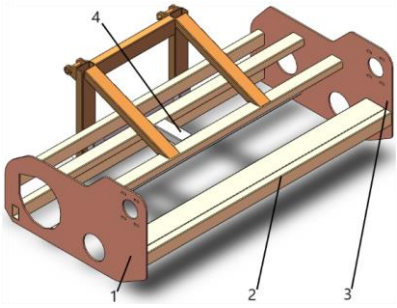

Fig. 1 - Simplified frame for pickup header

1.Right side panel of the frame; 2.Frame front beam; 3.Left side panel of the frame; 4.Frame rear beam.

Save the simplified 3D model of the frame in STP format and import it into ANSYS(19.0). The model's material properties are defined as Q235 steel, featuring an elastic modulus of 210 GPa, a Poisson's ratio of 0.3, and a density of 7850 kg/m^3. Subsequently, the model was meshed with an element size of 5 mm. Upon completion of the meshing process, it yielded a total of 668,922 nodes and 315,187 elements.

The header vibration test

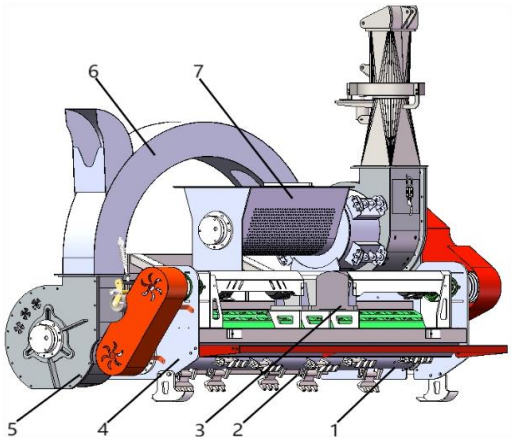

Fig. 2 - Straw forage harvester pick up header

1. Hammer Claw Device; 2. Conveying device; 3. Transmission; 4. Right side panel of the frame; 5.Conveyor box; 6. Ejection device; 7. Dust box.

This study focuses on the straw forage harvester pickup header (shown in Figure 2), analysing the vibration contribution of primary excitation sources (such as the hammer claw, conveying auger, dust removal systems, and transmission) at various engine speeds, transmitted through their respective paths to the pickup header frame during harvester downtime. To eliminate interference from external excitations during the analysis of the main excitation sources, the experiment was performed in a controlled stationary vibration test environment on a paved surface for the straw feed harvester. The experiment took place at the Hongchang Machinery Factory, located in Hohhot, Inner Mongolia Autonomous Region, China. The experimental conditions are designed based on engine speed, which ranges from 1000 r/min to 2000 r/min, increasing by 200 r/min for each condition. This results in a total of six different conditions, with each condition being tested for a duration of 60 seconds. The experimental condition corresponding to an engine speed of 1600 r/min is designated as the target response condition. The remaining conditions are used to establish a condition transfer path analysis model.

Prior to the experiment, the DH5902N data acquisition instrument from Donghua Testing Company was selected, with a sampling frequency set to 2.56 kHz. Subsequently, triaxial accelerometers were positioned near the excitation sources. The positive X direction of the accelerometers was aligned with the forward direction of the pickup cutter bed, the positive Y direction was set vertically upward from the ground, and the Z direction represented the transverse motion of the pickup cutter bed, with its positive direction defined by the right-hand rule.

The distribution of measurement points on the pickup header is detailed in Table 1.

Figure 3 shows the installation diagram of these measurement points on the straw forage harvester's pickup header, and Figure 4 provides the schematic diagram of the vibration test setup for the straw forage harvester.

(a) (b) (c)

Fig. 3 - Header frame part measurement point

(a) Right side panel of the frame; (b) Transmission; (c) Left side panel of the frame.

Fig. 4 - Field test of straw feed harvester

Table 1

Pickup header frame measuring point layout table

Response Points	Positions	Measurement point	Positions
1	Right side panel of the frame	2	Hammer-claw drive shaft
		3	Transmission right output shaft
		4	Conveyor box end
5	Left side panel of the frame	6	Transmission left output shaft
		7	Conveyor drive shafts
		8	Dust box drive shaft
10	Frame front beam	9	Transmission input end
12	Frame rear beam	11	Dust box end

Establishment and validation of the OTPA model for the pickup header

Operational Transfer Path Analysis (OTPA) method

The OTPA method is an enhancement of the traditional Transfer Path Analysis (TPA) method. Its model utilizes an 'input-transfer path-output' representation to analyse vibrations in mechanical systems (*Xia et al., 2021; Liao et al., 2021*). The theoretical formula for OTPA is:

$$P(\omega)=\sum_{j=1}^{m}T_j(\omega)P_j(\omega)+\sum_{i=1}^{m}TT_i(\omega)Q_i(\omega) \quad (1)$$

where: P represents the vibration at the target point; ω represents the excitation frequency of the signal; TT_i $(i=1,2,\ldots,n)$ denotes the transfer function of the vibration signal from the iiith position to the target point; Q_i represents the vibration response signal at the i^{th} position, characterized by the root mean square value of acceleration measured at the point; P_j represents the acoustic pressure response signal at the j^{th} position.

In practical applications, the vibration signals from different excitation sources are integrated into the input signal matrix X, and the response data of the target point are integrated into the output matrix Y. The transfer function matrix T is used to reflect the relationship between the input signals and the output responses. Where $Y=X\cdot T$. It follows that:

$$T=\left(X^TX\right)^{-1}X^TY=G_{XX}^{-1}G_{XY} \quad (2)$$

where: G_{XX} represents the auto power spectrum of the input signal; G_{XY} represents the cross power spectrum between the input signal and the output signal.

In the field of engineering, signals are often affected by noise and crosstalk. Therefore, to avoid interference between input signals, the technique of truncated Singular Value Decomposition (SVD) is introduced into the computational process. The new mathematical expression for the vibration system then becomes:

$$X_{\text{real}}T = Y_{\text{Ture}} + \varepsilon = Y \tag{3}$$

where: X_{real} represents the input matrix of excitation data obtained from actual measurements; ε represents the small error amount caused by coupling and crosstalk among the measured input signals; Y_{Ture} represents the true output of the system under ideal conditions; Y represents the output values of the system obtained from measurements.

Assuming the number of system inputs is n and the number of operating conditions is s, the signal matrix is subjected to Singular Value Decomposition (SVD), as shown in equation (9):

$$X_{\text{real}} = U\Sigma V^T \tag{4}$$

where: U is an $s \times s$ unitary matrix; V is an $n \times n$ unitary matrix; Σ in an $s \times n(s \geq n)$ diagonal matrix.

This can be represented by equation (10):

$$\Sigma = \text{diag}(\sigma_1, \sigma_1, \ldots, \sigma_n) \tag{5}$$

where: $\sigma_1 \geq \sigma_2 \geq \cdots \geq \sigma_n \geq 0$. Connecting equations (2-8) to (2-10), the transfer function matrix T can be expressed as:

$$T = \sum_{i=1}^{n} \left(\frac{u_i^T \left(Y_{\text{Ture}} + \varepsilon \right)}{\sigma_i} \right) v_i \tag{6}$$

where: u_i and v_i are the ith column vectors of the unitary matrices ∪ and V, respectively.

The contribution of the i^{th} input to the j^{th} output through the transfer path is:

$$Y_{i,j}^{\text{contri}} = X_i Y_{i,j} \tag{7}$$

The formula for calculating the contribution rate of singular values is:

$$CR = \frac{\sigma_i}{\sum_{i=1}^{n} \sigma_i} \times 100\% \tag{8}$$

In matrix decomposition, truncation of smaller singular values is commonly employed to ensure the stability of the inversion operation. The truncated singular value matrix is denoted as $\bar{\Sigma}$ and the formula for calculating the transfer matrix is:

$$\bar{T} = \bar{X} + Y = V\bar{\Sigma}^{-1}U^T Y = \sum_{i=1}^{n-l} \frac{u_i^T Y}{\sigma_i} v_i \tag{9}$$

Establishment of the OTPA model

The modal analysis and vibration testing of the pickup header indicate that the primary deformation areas of the pickup header frame are the side panels and the front and rear over-bridge sections. Consequently, measurement points 1, 5, 10, and 12 were positioned on the left and right sides, as well as the front and rear bridge beams of the pickup cutter bed frame, serving as model response points. The remaining measurement points were positioned on the operational components of the cutter bed frame, serving as model excitation points. Under the target condition of 1600 r/min, a 4×8 OTPA model was developed, as illustrated in Figure 5.

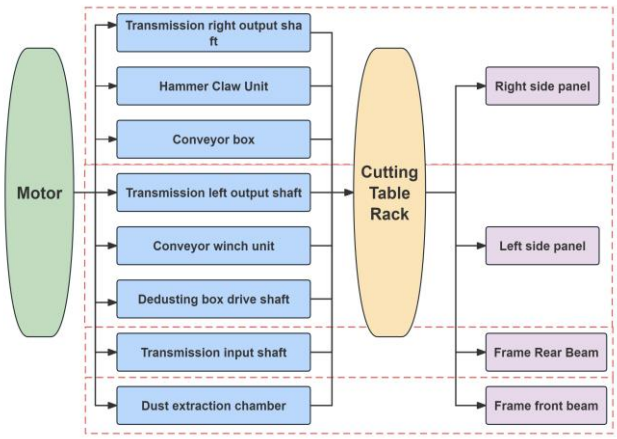

Fig. 5 - Pick up header OPTA vibration transmission path diagram

Validation of the OTPA model

The established OTPA model requires validation for source leakage detection. Typically, the coherent function is utilized to verify if the model output is induced by the model input and to identify any significant missing transfer paths.

According to the Multiple-Input Single-Output（MISO）system, the relationship between inputs and outputs can be expressed as follows:

$$S_{yy} = S_{vv} + S_{ee} \tag{10}$$

where: S_{yy} represents the auto power spectrum of the output signal; S_{VV} represents the portion of the output signal power spectrum caused by the input signal; S_{ee} represents the portion of the output signal power spectrum caused by non-input signals (noise, unreferenced excitations, system errors, etc.).

Therefore, the cross-correlation function of the system can be expressed as:

$$\varsigma_{y.x}^2 = 1 - \frac{S_{ee}}{S_{yy}} \tag{11}$$

In practical engineering, it is desirable for the coherence function value to be as high as possible, and it typically needs to satisfy a coherence function value $\varsigma_{y\cdot x}^2 \geq 0.6$ *(Zheng, and Qian et al., 2016)*.

According to Equation (11), the vibration data under the target operating condition is processed to validate the established OTPA model, yielding the coherent function of the system under this condition. The results are shown in Figure 6:

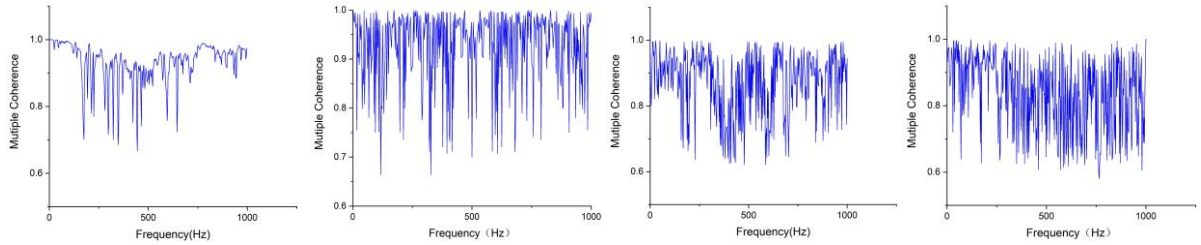

(a) (b) (c) (d)

Fig. 6 - Recoherence function of header vibration model

(a). Model re-coherence function for vibration on the right side of the frame; (b). Model re-coherence function for vibration on the left side of the frame; (c). Model re-coherence function for frame front beam vibration; (d). Model re-coherence function for frame rear beam vibration.

As illustrated in the figure, the coherence function values between the input and output signals under the target operating conditions are generally above 0.6, thereby meeting the engineering requirement of 0.6. This indicates that the primary excitation sources of the model output signals originate from the vibrations observed at the measurement points, with no significant excitation sources or transfer paths omitted. Thus, the vibration data from the specified excitation and response points can be utilized to develop a model for analysing the transfer paths under these operating conditions.

RESULTS AND DISCUSSION

Modal analysis

Taking into account the actual working conditions of the pickup cutter bed, a modal analysis was performed on the pickup cutter bed in a free state. The model imposed no constraints on the translational and rotational degrees of freedom in the X, Y, and Z directions. The first six non-zero modal frequencies and corresponding mode shapes were calculated and analysed. Utilizing ANSYS Workbench(19.0), the first six natural frequencies and mode shape contour plots of the pickup header frame were obtained. The simulation results are shown in Figure 7, and the frequencies and mode shapes of each order are listed in Table 2.

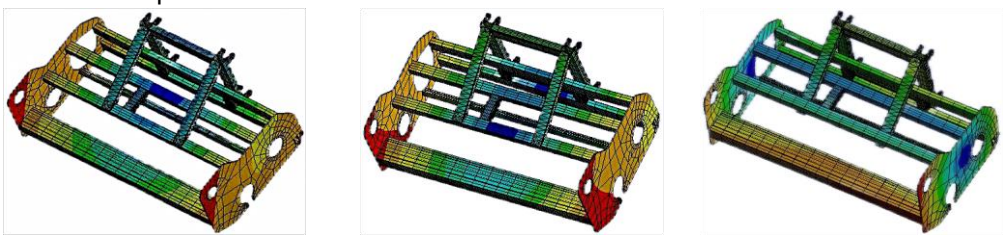

a) *Frist-order modal*) b) *Second-order modal*) c) *Third-order modal*

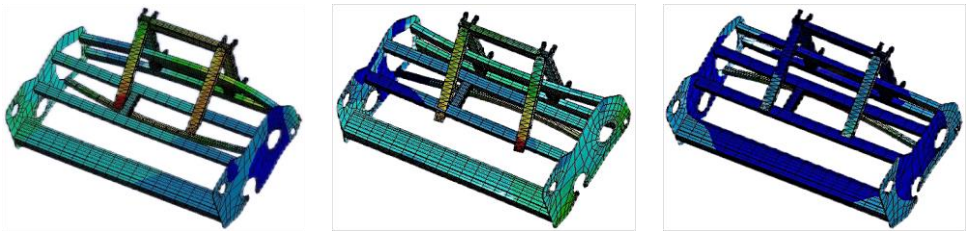

d) *Fourth-order modal* e) *Fifth-order modal* f) *Sixth-order modal*

Fig. 7 - The front sixth-order modal shapes of the pickup header frame

Table 2

Modal results of finite element analysis

Modal order	Frequency/Hz	Modal shape characteristics
1	8.3284	Bending of left and right side panels along the z-axis
2	9.7012	Torsion of the front beam along the z-axis
3	15.549	Torsion of the rear beam along the z-axis
4	29.959	Torsion + bending of rear beam along z-axis
5	32.741	Torsion + bending of right beam and right side panel along z-axis
6	35.624	Torsion + bending of the frame along the z-axis

The detailed results of each mode from the finite element modal analysis are presented in Table 2. The first six modes include both bending and torsional modes. The first six natural frequencies of the pickup header frame range from 0 to 40 Hz. The fourth, fifth, and sixth natural frequencies are relatively concentrated between 30 and 35 Hz. The corresponding vibration modes involve the torsion and bending of the left and right side panels as well as the front and rear cross beams. When external excitations fall within the 30 to 35 Hz range, resonance may occur in the frame, resulting in overall torsion and bending deformation of the structure.

Time-domain analysis of experimental results

The intensity of cutter bar vibration is a key indicator for assessing the operational condition of agricultural machinery. Using the root mean square (RMS) value of vibration acceleration to measure vibration intensity effectively reflects the amplitude and energy intensity of the structure.

The calculation is shown in Equation (12):

$$\mathrm{RMS} = \sqrt{\frac{1}{N}\sum_{k=1}^{n} x^2{}_{\mathrm{k}}} = \sqrt{\frac{x_1{}^2 + x_2{}^2 + x_3{}^2 + \cdots + x_k{}^2}{N}} \quad (12)$$

In the equation: x_k represents the vibration signal; N is the number of trials.

The vibration acceleration signals collected from the belt are processed to extract the root mean square values of the acceleration from the time-domain signals recorded at the measurement points. The specific values for the 12 measurement points on the harvester frame are shown in Figure 8.

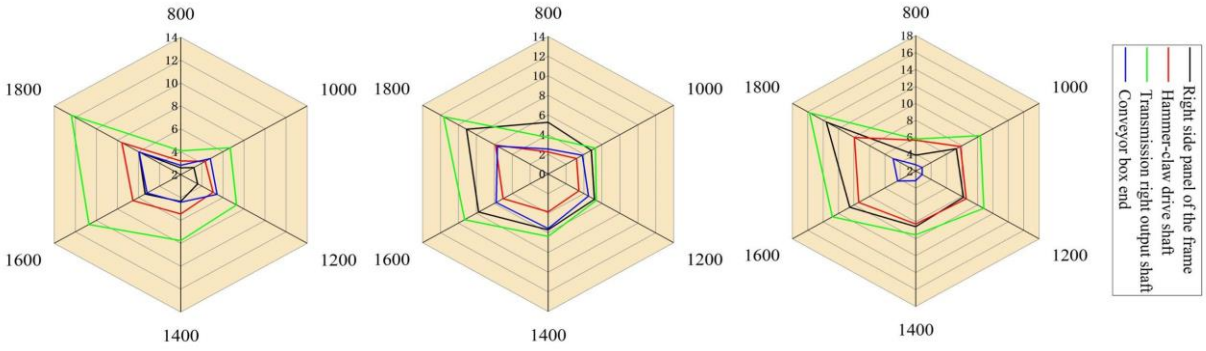

（a）Rack right side X-direction （b）Rack right side Y-direction （c）Rack right side Z-direction

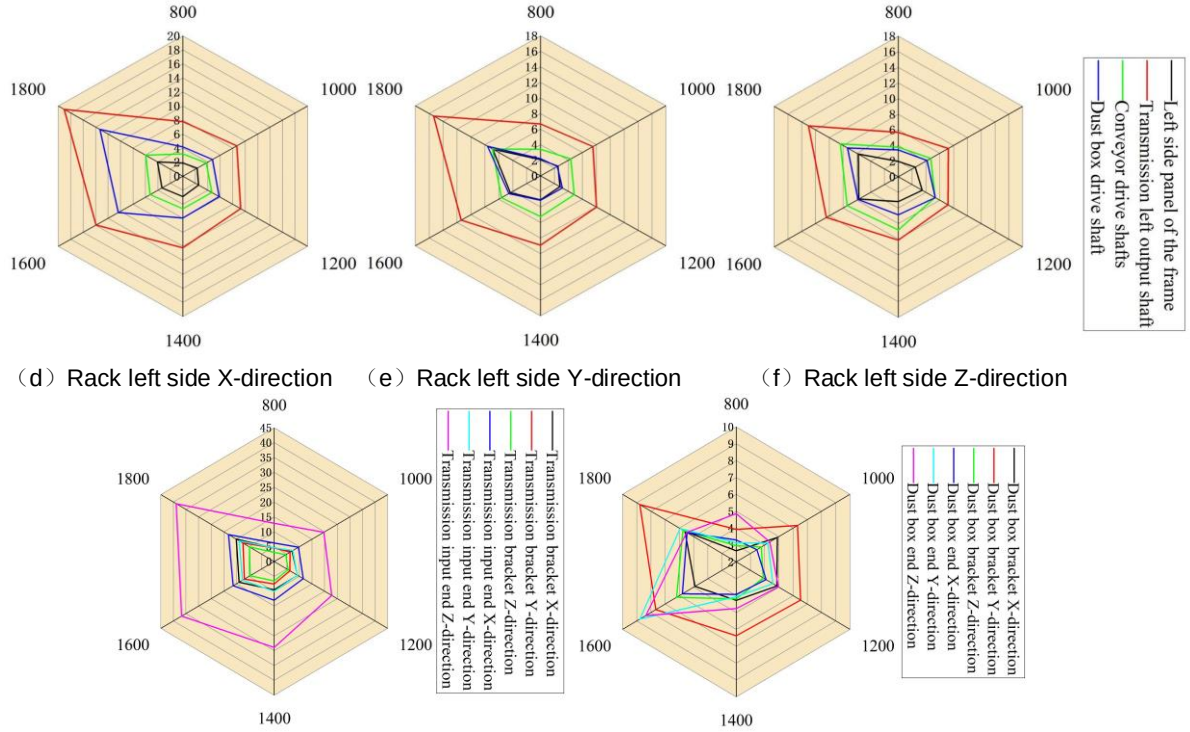

（d）Rack left side X-direction （e）Rack left side Y-direction （f）Rack left side Z-direction

（g） Rack Front Beam （h） Rear frame beam

Fig. 8 - Root mean square value of vibration acceleration of measuring points under different working conditions of frame

(a ~c) Root-mean-square value of vibration acceleration at the right side of the frame. (d ~f) Root-mean-square of vibration acceleration at the left measurement point of the rack. (g) Root-mean-square value of vibration acceleration at measurement points on the front beam of the frame. (f) Root-mean-square value of vibration acceleration at the rear beam measurement point of the frame.

Analysis of acceleration signals at multiple vibration measurement points under varying operating conditions indicates a consistent upward trend in vibration magnitude in the X, Y, and Z directions as engine speed increases. At the target operating speed of 1600 r/min, the RMS value of vibration acceleration for the entire header frame shows a significant increase. This suggests that under these conditions, the excitation frequency from a specific source closely aligns with the header frame's natural frequency, resulting in a resonance effect.

Analysis of the vibration responses of the right side plate of the header frame to various excitation sources under different operating conditions indicates that the vibration amplitude at the right output shaft end of the transmission (measurement point 3) is consistently higher in all three axes compared to other measurement points. The difference in vibration amplitudes is most pronounced at the target operating speed of 1600 r/min, suggesting that the vibrations on the right side of the header frame are predominantly due to excitation from the rotational motion of the transmission's right output shaft. Further analysis reveals that the vibration excitation in the Z-axis at the drive shaft end of the hammer claw device (measurement point 2) is particularly pronounced. This finding suggests that during the operation of the pickup header, the excitation from the hammer claw device primarily influences the transverse vibration of the header frame's right side plate. The analysis results indicate that the primary sources of vibration affecting the right side of the header frame, ranked by impact, are the transmission right output shaft (measurement point 3), the hammer claw device (measurement point 2), and the conveyor housing (measurement point 4).

Comparison of the vibration responses from various excitation sources on the left side of the harvester frame under different operating conditions reveals that the vibration amplitudes at the left output shaft end of the transmission (measurement point 6) in the X, Y, and Z directions exceed those at other measurement points. This trend is further accentuated at the target operating speed of 1600 r/min. This finding suggests that the predominant factor influencing vibration on the left side of the harvester frame is the vibrational excitation from the rotational movement of the transmission's left output shaft end. Under each operating condition, the vibrational excitation at the drive shaft end of the dust removal device (measurement point 8) in the X-direction is notably prominent. This suggests that the dust removal device has a significant impact on the vibration of the harvester frame's left side plate in the longitudinal direction during operation. This is likely due to the fact that the excitation generated by the operation of the dust removal device primarily propagates along the X-axis.

A comprehensive analysis reveals that the main excitation sources influencing the vibration of the left side plate of the harvester frame, ranked from strongest to weakest, are the left output shaft of the transmission (measurement point 6), the dust removal device (measurement point 8), and the conveying auger device (measurement point 7).

Analysis of the vibration responses of the header frame front beam under various operating conditions shows that the vibration amplitude at the transmission input end in the horizontal direction exceeds those in other directions. This suggests that the primary influence on the vibration of the header frame front beam is the horizontal vibration excitation originating from the transmission input end. At the target operating speed of 1600 r/min, significant changes in the vibration amplitudes are observed for both the header frame front beam and the transmission input end. This observation suggests that resonance coupling between the transmission input end and the front beam may occur under this test condition.

Analysis of the vibration responses of the header frame rear beam under various operating conditions clearly shows that the vibration amplitudes at the dust box end are significant in both the horizontal and vertical directions. At the target operating speed of 1600 r/min, there is a considerable sudden increase in vibration amplitude. At the same operating speed of 1600 r/min, the vibration amplitude of the header frame rear beam significantly increases in both horizontal and vertical directions. This observation suggests that at this operating speed, the excitation from the dust collector box may resonate with a particular natural frequency of the frame's rear beam.

In summary, the pickup header undergoes varying degrees of vibrational deformation on both the left and right sides of the frame, as well as at the front and rear beams, due to multiple excitation sources. At the target operating speed of 1600 r/min, the impact on the frame is particularly significant, aligning with the results of the modal analysis of the cutting table frame.

Frequency domain analysis of experimental results

The time-domain signals from vibration tests at various measurement points on the pickup header were analysed using Fast Fourier Transform (FFT). A total of 2048 analysis points were selected, with a rectangular window applied, and amplitude correction was performed on the window. This process produced the frequency spectrum characteristics for each measurement point. The frequency amplitude table is shown in Table 3:

Table 3

The vibration frequency and amplitude of the main excitation source in the target condition

Measurement point	Peak number	X-direction		Y-direction		Z-direction	
		Frequency / Hz	Amplitude / m*s^{-2}	Frequency / Hz	Amplitude / m*s^{-2}	Frequency / Hz	Amplitude / m*s^{-2}
2	1	408.7	1.492	33.75	4.9	175	1.724
	2	33.75	1.367	476.8	2.476	183.75	1.526
	3	443.1	1.239	408.7	2.417	170.625	1.435
3	1	613.1	2.541	33.75	2.437	183.7	3.042
	2	31.75	2.39	443.1	1.388	170.6	1.771
	3	647.5	2.159	609.3	1.264	158.7	1.29
4	1	183.7	1.55	34.3	2.437	183.7	3.042
	2	338.7	1.122	443.1	1.388	170.6	1.771
	3	341.8	1.004	91.8	1.264	158.7	1.29
6	1	44.3	4.427	960	2.085	449.3	5.16
	2	960	2.49	933.1	1.936	35.85	2.486
	3	946.8	1.906	42.5	1.726	483.7	2.064
7	1	771.8	1.891	449.3	2.198	414.3	2.319
	2	763.8	1.125	791.2	1.128	771.8	1.891
	3	733.1	0.959	763.7	1.081	483.7	1.746
8	1	449.3	4.817	485.6	1.527	449.7	1.342
	2	480.6	3.129	481.2	1.326	480.6	0.903
	3	476.8	2.669	491.2	1.065	617.5	0.855
9	1	451.2	9.153	901.8	3.205	798.1	11.778
	2	69.375	3.749	901.7	2.984	34.75	10.145
	3	277.5	2.537	416.25	2.979	867.5	9.881
12	1	849.3	1.699	849.3	5.47	755	4.061
	2	69.3	1.154	416.2	3.09	759.3	1.894
	3	35	1.054	63.125	1.067	647.5	1.43

The vibration frequency at the transmission output shaft is primarily determined by the rotational speed of the power output shaft. The vibration frequency of the hammer claw device is primarily determined by the frequency at the drive pulley. The vibration frequency of the conveyor box is primarily determined by the frequency at the conveyor shaft bearing cover. As shown in Table 3, the vibration amplitude of the hammer claw device is the largest, reaching up to 4.9 $m*s^{-2}$ in the Y-direction (vertical direction). This is because the hammer-claw drive shaft is the first component to come into contact with the straw, leading to significant variations in vibration amplitude. The frequently occurring vibration frequencies at Measurement Points 2, 3, and 4 in the X and Y directions—33.75 Hz, 31.75 Hz, 34.3 Hz, and 91.8 Hz—are closely aligned with the fundamental and harmonic frequency range of the header frame's natural frequency, which is between 29 and 35 Hz. This proximity makes it prone to resonance coupling phenomena.

The vibration frequencies of the conveying device and the dust box are primarily dominated by the fundamental and higher frequencies of the drive pulley. As can be seen from Table 3, the vibration amplitude at the transmission's left output shaft is higher than that of the conveying device and dust box, with the greatest amplitude occurring in the Z-direction (horizontal direction), reaching up to 5.16 $m*s^{-2}$. Additionally, the frequencies occurring in all three directions at the transmission's left output shaft—44.3 Hz, 42.5 Hz, and 35.85 Hz—are close to the sixth-order natural frequency of the frame, making it susceptible to frame resonance coupling phenomena.

The vibration frequency at the transmission input end is caused by the engine speed, with a notably significant vibration amplitude in the Z-direction (horizontal direction). The maximum amplitude reaches 11.778 $m*s^{-2}$. This is due to the triangular configuration of the transmission's input and output shafts. Among these, the frequency of 69.4 Hz in the X-direction falls within the double frequency range of the sixth-order natural frequency of the frame, and the frequency of 34.75 Hz in the Z-direction is close to the fifth-order natural frequency of the frame. These conditions are likely to cause resonance coupling between the transmission and the front beam of the header frame.

Measurement Point 11, located at the dust box end, exhibits a vibration amplitude in the Y-direction (vertical direction) that is higher than in other directions, with the maximum vibration amplitude reaching 5.47 $m*s^{-2}$. Among these, the frequencies of 69.3 Hz, 63.1 Hz, and 35 Hz occurring in the X- and Y-directions fall within the fundamental and double frequency range of the sixth-order natural frequency of the frame. Therefore, these frequencies are likely to cause resonance coupling in the frame.

Comparing the excitation frequencies with the modal parameters of the header frame reveals that Measurement Points 2, 3, 6, 9, and 12 all have frequencies within the fundamental and harmonic frequency range of the header frame's natural frequencies, which is between 30 and 35 Hz. Therefore, when the straw forage harvester is operating normally, excitation sources such as the hammer claw device, transmission, conveyor box, and dust box can induce resonance in the header frame. Consequently, it is necessary to analyse the vibration transmission paths and contribution levels from each excitation source to the response points on the header frame.

Analysis of transmission path results under operating conditions

According to the principles of the Operational Transfer Path Analysis (OTPA) method, establishing a model requires constructing an input signal matrix and a corresponding target response point matrix. The experimental data under the target conditions were processed and analysed according to Equation (9). The synthesized vibration data from the model response points were then compared with the actual measured data, with the results shown in Fig. 9.

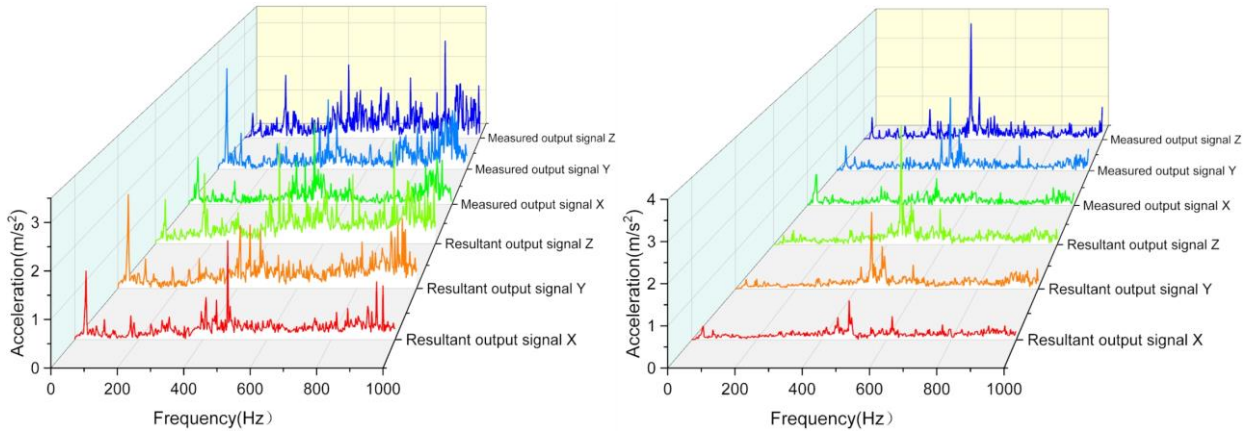

(a) (b)

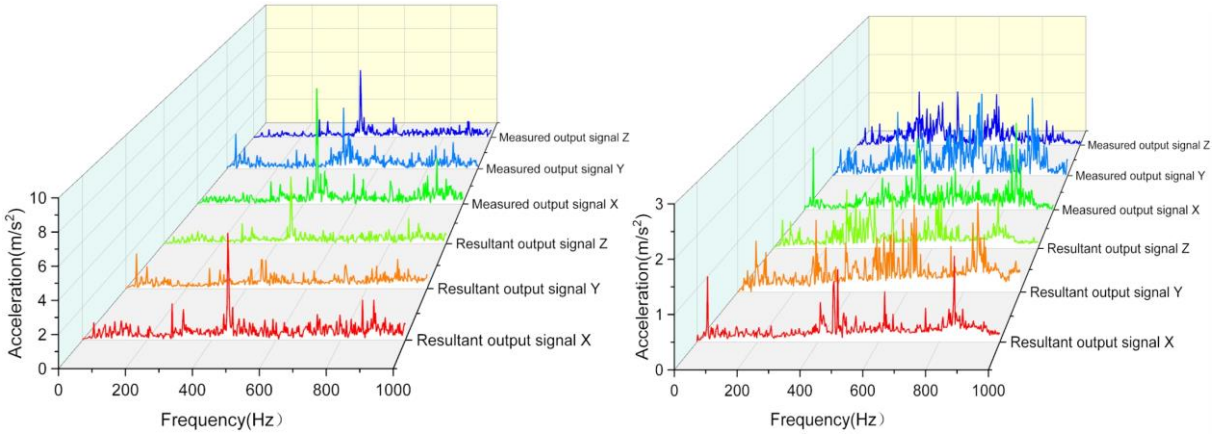

Fig. 9 - Comparison between the synthetic signal and the measured signal

(a) Rack right hand side working condition transfer path analysis model; (b) Rack left hand side working condition transfer path analysis model; (c) Frame front beam working condition transfer path analysis model; (d) Frame rear beam working condition transfer path analysis model.

As demonstrated in Figure 9, the output signal synthesized by the OTPA model closely matches the measured signal. The model displays consistent magnitude and variation trends within the analysis frequency band, effectively capturing the vibration transmission from various excitation sources on the straw forage harvester's pickup header to the designated response points on the header frame.

Building on this foundation, the validated model for operational condition transfer path analysis can be employed to determine the vibration contributions of each measurement point to the response points on the header frame at the characteristic frequencies under specified operational conditions, as outlined in Equation (7). By analysing the contribution of each transfer path to the structural vibrations at characteristic frequencies under test conditions, the influence on the four response points of the pickup header is determined, as illustrated in Figure 10.

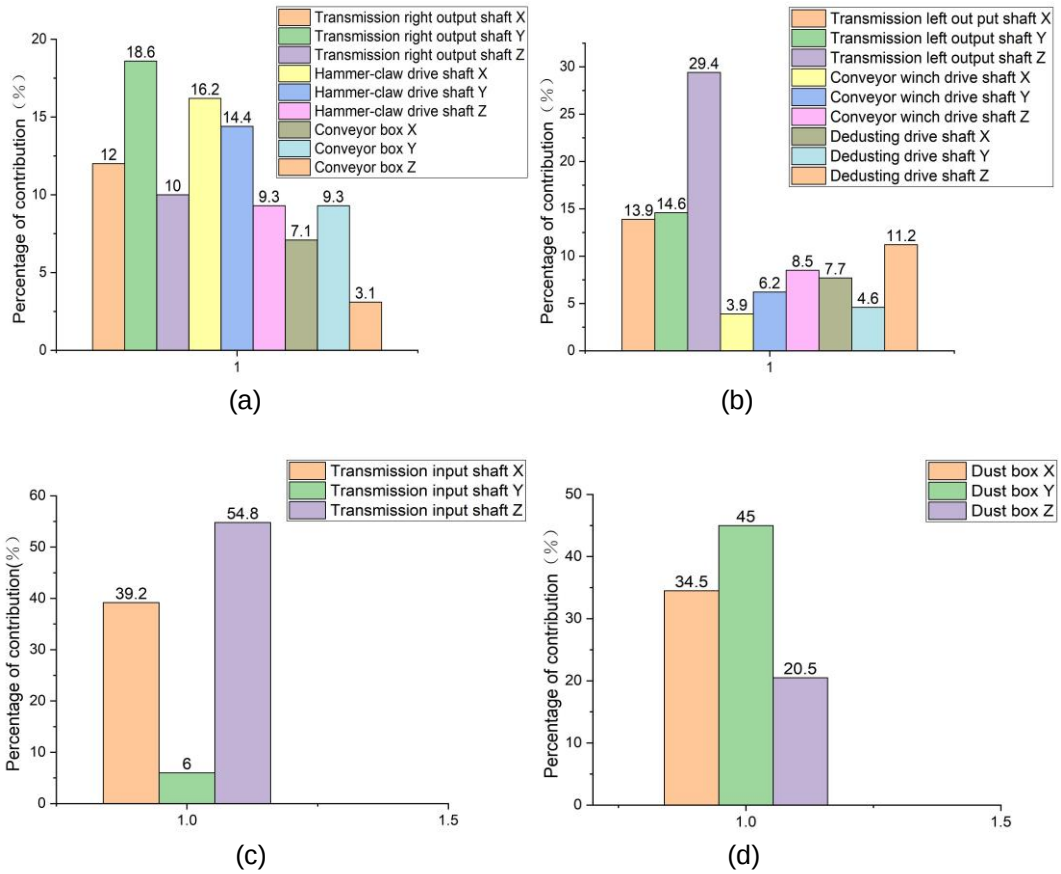

Fig. 10 - Characteristic frequency points of each path contribution diagram

(a) Excitation vibration contribution from the right side of the frame; (b) Excitation vibration contribution from the left side of the frame; (c) Excitation vibration contribution from the front beam of the frame; (d) Excitation vibration contribution from the rear beam of the frame.

Analysis of the vibration contribution diagram for the right side of the frame indicates that the transmission output end and the hammer-claw drive shaft are the primary contributors to the vibration on the right side of the header, accounting for 40% and 39% respectively. The primary contributors to vibration on the right side of the frame are: the transmission output end, accounting for 18.58% of the vertical vibrations; and the hammer-claw drive shaft, which contributes 16.24% to forward vibrations and 14.35% to vertical vibrations. Observations indicate that the largest contributions to the forward and vertical directions of the right side panel of the pickup header frame come from various transfer paths, whereas the lateral contributions are the smallest. Therefore, in optimizing vibration reduction for the pickup header, priority should focus on the forward and vertical directions of the frame's right-side panel.

Analysis of the vibration contribution diagram for the left side of the frame shows that the transmission output end accounts for a significant 57.89% of the vibrations, markedly more than the other two measurement points. The transmission output end is the most significant contributor to the horizontal vibrations of the frame's left side, accounting for 29.41%. This observation reveals that excitation sources contribute predominantly to the lateral vibrations of the left side panel of the pickup header, with the smallest contribution in the forward direction. Therefore, in optimizing vibration reduction for the pickup header, particular emphasis should be placed on mitigating the impact of the gearbox output shaft end on the lateral vibrations of the left side panel.

Analysis of the vibration contribution diagram for the frame's front beam indicates that the transmission input end primarily contributes to vibrations in the forward and horizontal directions of the header, accounting for 39.2% and 54.8% respectively. The primary vibration contributions from the transmission input end are in the Z, X, and Y directions, respectively. This indicates that the excitation sources predominantly affect the front beam of the pickup header in the forward and horizontal directions. Consequently, in optimizing vibration reduction for the front beam of the pickup header, particular emphasis should be placed on mitigating the transmission's impact on the forward and horizontal directions.

The analysis of the vibration contribution diagram for the frame's rear beam reveals that the dust box end primarily contributes to vibrations in the forward and vertical directions of the header, accounting for 45% and 34.5% respectively. At the dust box end, the vibration contributions are ordered as follows: Y-axis, X-axis, and Z-axis. This analysis shows that the excitation source contributes most significantly to the vertical vibrations of the pickup header's rear beam, and least to the horizontal vibrations. During the vibration damping optimization for the rear beam of the pickup header, emphasis should be placed on mitigating the impact of excitation from the dust box in the vertical direction.

In summary, during operation, the pickup header of the straw forage harvester is primarily influenced by excitations from the power input shaft, the left and right output shafts of the transmission, the hammer-claw drive shaft, and the dust box. These influences are specifically manifested in the forward and vertical vibrations of the header frame's right side plate, the horizontal vibrations of the left side plate, and the forward and horizontal vibrations of the front beam, as well as the vertical vibrations of the rear beam.

CONCLUSIONS

This study focuses on the pickup header of a straw forage harvester. By integrating modal analysis, vibration testing, and operational transfer path analysis, the vibration characteristics of the pickup header frame and its excitation sources were identified. Additionally, the primary transfer paths and their contribution levels to the vibration of the pickup header were identified. The key findings are as follows:

(1) The vibration characteristics of the pickup header frame are as follows: the primary response areas to excitation sources are located on the left and right sides, as well as the front and rear beams of the frame. Additionally, the excitation frequencies of sources like the hammer claw device, transmission output shaft, transmission input shaft, and dust box closely match the natural frequencies of the pickup header, potentially causing resonance coupling.

(2) The study examined the feasibility of using the Operational Transfer Path Analysis (OTPA) method, based on Singular Value Decomposition (SVD), to analyse the transmission paths of vibrations from excitation sources to the frame of the straw forage harvester's pickup header. An OTPA model was developed to map excitation points to response points. The model's accuracy was validated by comparing the agreement between simulated synthetic signals and measured signals within the study frequency range. This provides a theoretical basis for the structural optimization of the pickup header.

(3) The main transmission path contributions are as follows: For the right side panel of the frame, the primary contributors are the transmission's right output shaft (vertical direction) and the hammer-claw drive shaft (forward and horizontal directions). For the left side panel of the frame, the primary contributor is the transmission's left output shaft (horizontal direction). For the front beam of the frame, the primary

contributor is the transmission's input shaft (forward and horizontal directions). For the rear beam of the frame, the primary contributor is the dust box end (forward and vertical directions).

In summary, this study has identified the fundamental causes of vibration deformation in the pickup header of the straw forage harvester. This provides crucial insights for optimizing vibration reduction and structural design in new models of the pickup header, offering valuable references for the development of other agricultural equipment as well. Moreover, it provides a theoretical basis and new perspectives for optimizing vibration reduction and structural design, with potential applications in multi-source excitation load studies and vibration improvements for other electromechanical products.

ACKNOWLEDGEMENTS

We acknowledge that this work was supported by the National Natural Science Foundation of China (52365035), the Inner Mongolia Autonomous Region Science and Technology Programme (2022YFDZ0024), the National Natural Science Foundation of China (32071893), the Innovation and Entrepreneurship Training Programme for College Students of Inner Mongolia Agricultural University (202310129084) and the Priority Agricultural Engineering Projects (YLXKZX-NND-NYGCZD001).

REFERENCES

[1] Awad, Mahmoud, et al. (2022) A combined machine for collecting and chop rice straw. *Heliyon.* 8.8. https://doi.org/10.1016/j.heliyon.2022.e10412

[2] An, Xue, et al. (2020). Characterization of textural failure mechanics of strawberry fruit. *Journal of Food Engineering.* 282: 110016. https://doi.org/10.1016/j.jfoodeng.2020.110016

[3] Ahmadian, Hossein, Seyed Reza Hassan-Beygi, and Barat Ghobadian. (2014). Investigating a power tiller handle and seat vibration on transportation mode. *Agricultural Engineering International: CIGR Journal* 16.4: 194-206.

[4] Chen, Shuren, et al. (2020). Modal vibration response of rice combine harvester frame under multi-source excitation. *Biosystems engineering*. 194: 177-195. https://doi.org/10.1016/j.biosystemseng.2020.04.002

[5] Chuan-Udom, Somchai. (2017). Development of a cutter bar driver for reduction of vibration for a rice combine harvester. *Asia-Pacific Journal of Science and Technology* 15.7. 572-580.

[6] Chen Shuren, Han Hongyang, and Lu Qiang. (2012). Modal Analysis of Header for Type 4LZ 2. 0 Combine Harvester (4LZ-2.0 型联合收获机割台模态分析). *Transactions of the Chinese Society for Agricultural Machinery*, 43(S1): 90-94. https://doi.org/10.6041/j.issn.1000-1298.2012.S0.018

[7] Chen Jun-fei, et al. (2023). Transfer path analysis of product packaging system under random vibration (随机振动下产品包装系统传递路径分析). *Journal of Vibration Engineering*, 36(02): 507-516. DOI:10.16385/j.cnki.issn.1004-4523.2023.02.022. https://doi.org/10.16385/j.cnki.issn.1004-4523.2023.02.022

[8] De Klerk, Dennis, and Alexander Ossipov. (2010). Operational transfer path analysis: Theory, guidelines and tire noise application. *Mechanical systems and signal processing*. 24.7:1950-1962. https://doi.org/10.1016/j.ymssp.2010.05.009

[9] El Ghobashy, Hossam, et al. (2023). Development and evaluation of a dual-purpose machine for chop and crushing forage crops. *Heliyon.* 9.4. https://doi.org/10.1016/j.heliyon.2023.e15460

[10] Guo, Rong, et al. (2015). A novel visual transfer path analysis method with coupled vibration source based on inverse substructuring technique. https://doi.org/10.11908/j.issn.0253-374x.2015.04.015

[11] Harikrishnan, P. M., and Varun P. Gopi. (2017). Vehicle vibration signal processing for road surface monitoring. *IEEE Sensors Journal*. 17.16: 5192-5197. https://doi.org/10.1109/JSEN.2017.2719865

[12] Jiang, Yajun, et al. "Vibration analysis and improvement for frame of 4SY-2.9 typed rape windrower." Transactions of the Chinese Society of Agricultural Engineering 33.9 (2017): 53-60. https://doi.org/10.11975/j.issn.1002-6819.2017.09.007

[13] Lu, Wang, et al. (2014). Classification and comparison of physical and chemical properties of corn stalk from three regions in China. *International Journal of Agricultural and Biological Engineering*. 7.6: 98-106. https://doi.org/10.3965/j.ijabe.20140706.012

[14] Liao Xuhui, et al. (2021). Improved operational transfer path analysis (改进的工况传递路径分析). *Journal of Vibration and Shock*, 40(12):196-202+218. https://doi.org/10.13465/j.cnki.jvs.2021.12.024

[15] Lai, Z. N., S. Yang, and P. Wu. (2018). Speed-throttling combined optimization for high reliability in parallel centrifugal pump system. *Journal of drainage and irrigation machinery engineering*. 36.12: 1205-1210.

[16] McKendry, Peter. (2002) Energy production from biomass (part 2): conversion technologies. *Bioresource technology* 83.1: 47-54. https://doi.org/10.1016/S0960-8524（01）00119-5

[17] Nakata, Toshimichi, Yuji Sogabe and Takao Araki. (2010) Vibration property of a rubber crawler system when traveling over bumps. *Engineering in Agriculture, Environment and Food*. 3.2: 47-53. https://doi.org/10.11165/eaef.3.47

[18] QI Quan, et al. (2017). Structure-borne Noise Source Identification of an Excavator's Cab based on Operational Transfer Path Analysis (基于 OTPA 方法的挖掘机驾驶室结构噪声源识别). *Noise and Vibration Control*, 37(02): 80-84. https://doi.org/10.3969/j.issn.1006-1355.2017.02.017

[19] Xia, Erli, et al. (2021) A modified dynamic stiffness calculation method of rubber isolator considering frequency, amplitude and preload dependency and its application in transfer path analysis of vehicle bodies. *Applied acoustics*. 175: 107780. https://doi.org/10.1016/j.apacoust.2020.107780

[20] Yao, T. T., and Y. Zheng. (2020) Finite element analysis of stress, deformation and modal of head cover in axial-flow hydro-turbine. *Journal of Drainage and Irrigation Machinery Engineering* 38.1: 39-44. https://doi.org/10.3969/j.issn.1674-8530.18.0140

[21] Zheng Qi-ming, Qian Jing. (2016). Improvement of the Operational Transfer Path Model of a Label Sewing Machine Using Multiple Coherence Analysis (利用改进重相干分析改进订标机工况传递路径模型). *Noise and Vibration Control*, 36(03):169-173. https://doi.org/10.3969/j.issn.1006-1335.2016.03.035